Nonlinear control of boundary impedance in an acoustic waveguide

Yoav Vered [a], and Izhak Bucher [b]

Dynamics Laboratory, Faculty of Mechanical Engineering, Technion – Israel Institute of Technology, Haifa 3200003, Israel

Preprint

Published paper DOI: https://doi.org/10.1121/10.0007228

Keywords: Impedance tube; Adaptive control; Traveling waves; Extremum control;

[a] Electronic mail: V.Yoav@soton.ac.uk ; syoavv@technion.ac.il. Current address: Institute of Sound and Vibration Research, University of Southampton, Southampton SO17 1BJ, United Kingdom

[b] Electronic mail: bucher@technion.ac.il

Abstract

Wavetubes are employed for measurements of acoustic properties in various fluids. The ability to manipulate and control the frequency-dependent boundary impedance of the tube improves the estimation accuracy. Passive solutions, which use composite materials to change the boundary impedance, enable one to realize a finite combination of boundary impedances. In this paper, the tube boundary impedance is tuned at will by using two loudspeakers. The suggested method operates in the presence of dispersion by estimating, in real-time, a parametric reduced-order model using a multichannel least mean square algorithm. The identified model is fed to a nonlinear, adaptive control algorithm to realize modal traveling wave ratio control. It has been noted that the traveling wave ratio is smooth and parabolic across closed regions in the parameter space, thus assuring the convergence of the nonlinear control. Several methods to estimate the traveling wave ratio gradient are considered and compared based on an analytical model of a rigid impedance tube. An experimental case study utilizing an air-filled impedance tube with two loudspeakers is presented. The results demonstrate the ability to control the dynamics of the principal acoustic mode at will. Thus, enabling one to set the desired tube's boundary impedance.

I. INTRODUCTION

Wavetubes play an essential role in the conduction of nondestructive testing (NDT) of composite materials to measure their acoustic properties[1,2]. The wavetube comprises a hollow elastic cylinder filled with a representative fluid under which the acoustic properties are estimated. Usually, the material specimen is placed in the middle of the wavetube while two sets of microphones are located at each side of the specimen, a loudspeaker is placed at one of the tube's ends to generate the propagating pressure wave, and in most cases, an anechoic termination is placed at the other tube's end[3]. Most acoustic properties testing experiments separate the measured pressure wave into its forward and backward traveling components under the assumption of a single planar propagating mode[4]. It was shown[5–7] that the fluid pressure and the elastic tube interaction give rise to a rich dispersion diagram. The rich dispersion relation has at least two propagation modes (branches) at all frequencies[5–9]. Each of these modes is associated with different energy conveying mechanism[10]. It was also shown that such modes are excited in an air-filled thin plastic wavestube[7,11]. The contributions of the modes to the energy transfer are quantified by computing their modal power ratios[12]. Both the standing wave ratio (SWR)[13] and the traveling wave ratio (TWR)[14,15] can also be used to quantify the normalized amount and direction of energy transferred by each mechanism. It has been shown[16] that the power ratio and the TWR are equivalent descriptive parameters of the modal wave.

In several works[17–20], multiple excitation sources were considered and used to excite the pressure fields along the wavetube. While the classical work of Bodén and Holmberg et al.[18,19] considered a single propagation mode, in more recent work, Sack and Åbom[20] considered several propagation modes. In both cases, the importance of exciting different combinations of the

incident and reflected wave's amplitudes was emphasized[17]. If the acoustic sources' projections between various experiments do not differ, the sample's acoustic properties estimation becomes ill-conditioned[18]. Therefore, introducing the need to excite the wavetube in such a way will resolve in various wave's amplitudes. To this end, it is suggested here to use a model-based closed-loop control algorithm and to track the TWR reference signal of a prechosen mode, guaranteeing that the needed variety will be obtained.

The acoustic behavior along ducts and mufflers and its control are well-established fields. Several fundamental transcripts were published around 1980-2000, including the books by Munjal[21] and Nelson and Elliott[22]. In their book[22], Nelson and Elliott presented a thorough analysis of active noise control (ANC) of an air-filled duct under the assumption that the wave has a single nondispersive and planar mode. The ANC purpose is to attenuate the pressure at a region of the duct. This was achieved by introducing a second loudspeaker and tuning its time (phase) delay such that the superposition of the primary wave and the secondary wave sum to zero or that the pressure energy is minimal. Moreover, if the secondary loudspeaker is placed at the duct far end, they have shown that by tuning the secondary loudspeaker time delay to equal the propagation time along the duct, i.e., the duct length over the speed of sound, results in no reflection from the boundary, therefore, providing an effective anechoic termination. A secondary source was used in previous work to create an effective anechoic termination in wavetube for acoustic properties tests[23].

Although ANC of sound in ducts is known and implemented in many systems, changes to the classical methods should be introduced when considering dispersive waves and multiple modes[24,25], which are the outcome of an elastic fluid-filled tube[5,24]. In addition, if the control goal is not to attenuate the total pressure field or create an effective anechoic termination, a different

approach is needed. This work puts forward such an approach by decomposing the different dispersive modes and controlling the desired mode's TWR. By applying the proposed approach, the secondary actuator acts as an effective tunable impedance surface.

The TWR is preferable over the SWR or the power ratio as the reference signal since it is finite, bounded, and smooth[11,14]. Several methods to control propagation-related phenomena by applying traveling wave control[26] have been suggested in the past. Notable examples are the work of Mace[27], Minikes et al.[28], and Giraud et al.[29], which present control schematics for the traveling wave of a 1D beam. The work of O'Connor and Zhu[30], Habibi and O'Conner[31], and Peled et al.[32] dealing with the control of lumped parameter systems. The work of Gabai and Bucher[14], and Halevi[33] in which the 1D wave-equation governed systems were controlled. The work of Gabai and Bucher[34], Sirota and Halevi[35], Musgrave et al.[36], and Davis et al.[37] introduced control laws for systems governed by the 2D wave-equation. It was shown[14] that the open-loop model control is highly sensitive to model uncertainties; therefore, a model-based estimation closed-loop control should be used.

To track the modal TWR reference signal in real-time, an online model estimation is proposed. In previous work[38], a batch multichannel (MC) least-squares (LS) method was used to control the traveling wave in an air-filled impedance tube using an offline minimization implemented in MATLAB©. It was shown[11] that the MC least-mean-squares (LMS) [39] method is preferable over the MC recursive-least-squares[39] and the synchronous demodulation[11] methods for the recursive online decomposition of the measured pressure wave to its traveling wave components. The MC-LMS was implemented on a field-programmable gate array (FPGA), decomposing the pressure wave into its three dominant modes. As discussed previously[11], there is a need to decide the number of propagation modes to include in the model to minimize identification uncertainties. To

this end, an L-curve-based order selection regularization procedure[11,40,41] is used here at each frequency.

This work develops and verifies an adaptive control law capable of tracking a desired modal TWR reference signal. The verification includes both numerical simulation and an experimental study case. The preliminary experimental results of this research were presented and published during the 179th ASA meeting[42]. The current paper elaborates on the obtained results and puts forward an analytical model and numerical simulation on which the experimentation is based. The analytical model, from which the control law is derived, is developed and presented in Section II. The control law minimizes the squared tracking error function of the modal TWR by introducing a gradient descent adaptive control-law[43,44]. The stability of the control law is ensured by introducing a periodic extension of the parameter's domain. To estimates the TWR gradient, three methods are put forward. Namely, the finite difference approximation, the Extremum seeking[45], and the zero-order approximation. The methods are compared based on a numerical simulation that utilizes the analytical model to obtain the modal TWR for different values of parameters. The method convergence is analyzed based on the simulation results. The control derivation is presented in Section III.A. Each of the three methods to estimate the TWR gradient is described in Sections III.A.1, 2, and 3. The numerical simulation results and their analysis are presented in Section III.A.4. The adaptive MC-LMS method used to estimate the modal TWR recursively is described in Section III.B. Section IV shows the experimental results when applying the proposed control algorithm to an air-filled impedance tube at several excitation frequencies.

II. MODELING

A. Analytical model of an infinite-length fluid-filled elastic wavetube

The model being considered here is an infinite-length fluid-filled elastic wavetube with a circular cross-section. Previous papers presented the derivation and solution of analytical results for such a model[6,9]. In the current work, the analytical solution presented by Sato et al.[6] is adopted. The propagation direction in the current work is dubbed x and not z, and some minor changes in notation were made. Therefore, the obtained solution is revised here with appropriate notations. The fluids' complex velocity potential is denoted as ϕ_{f}, and it can be written using modal superposition. Each complex mode can be written as:

$$\phi_{\mathrm{f}(n,m)} = \mathrm{A}_{\mathrm{f}(n,m)} Z_n\left(\left|\eta_{(n,m)}\right| r\right) \mathrm{e}^{\mathrm{i}n\theta} \mathrm{e}^{\mathrm{i}\left(\omega t - k_{(n,m)} x\right)} + \mathrm{c.\,c.} \tag{1}$$

Here, ω and $k_{(n,m)}$ denote the wave angular frequency and modal wavenumber, $\mathrm{A}_{\mathrm{f}(n,m)}$ is the modal amplitude, (n,m) represents the modal order pair, $n = -\infty, \ldots, \infty$ denotes the azimuthal separation constant or the mode Fourier's coefficients, if $n \neq 0$ the mode comes in pair of $\pm n$, and $m = 1, \ldots, \infty$ denotes the radial separation coefficients order. $\eta_{(n,m)} \in \mathbb{C}$ denotes the set of radial separation coefficients, which are the zeros of the characteristic equation. Z_n represents the Bessel function of the first kind, J_n, if $\eta_{(n,m)}$ is nonnegative or otherwise, the modified Bessel function of the first kind, I_n. The modal wavenumber $k_{(n,m)} \in \mathbb{C}$ is a function of the angular velocity, the sound velocity of the fluid, v_{f}, and the appropriate radial separation coefficient, $\eta_{(n,m)}$, such that:

$$k^{\pm}_{(n,m)} \equiv \mp\sqrt{(\omega/v_{\mathrm{f}})^2 - \eta^2_{(n,m)}}, \tag{2}$$

where the plus and minus superscripts denote the forward and backward traveling directions.

Note that when the argument beneath the square-root is negative, i.e., $\eta_{(n,m)} > \omega/v_{\mathrm{f}}$, the modal wavenumber is purely imaginary and represents evanescent mode, which will decay along the wavetube. At each finite frequency, there exists only a finite number of real-valued modal wavenumbers, which are associated with propagation modes. For the elastic wavetube model, it is shown[46] that three modes propagate at low-frequency, namely two axisymmetric modes $(0,1)$ and $(0,2)$, and the first flexural mode $(\pm 1,1)$. Cutoff occurs at higher frequencies, where the square root argument of Eq. (2) becomes positive for additional modes. At the cutoff frequencies, additional modes start to propagate along the wavetube.

Therefore, up to the N^{th} cutoff, the complex pressure amplitude located at $\boldsymbol{r}_s = (x_s, r_s = R, \theta_s = 0)$, R being the tube inner radius, is given by:

$$P_{\mathrm{s}} = \sum_{\mu=1}^{N} J_{n_\mu}\left(\eta_{(n_\mu,m_\mu)}R\right)\left(P_\mu^+ e^{-\mathrm{i}k_\mu x_s} + P_\mu^- e^{\mathrm{i}k_\mu x_s}\right) + D.M., \tag{3}$$

where $P_\mu^\pm = \rho_{\mathrm{f}}\omega A_{(n_\mu,m_\mu)}^\pm$ denote the modal wave forward and backward complex amplitudes, *D.M.* denotes the double infinite summations over the decaying evanescent modes, and μ from now will be referred to the propagation mode number as well as the value of the modal order pair of the same mode for brevity. The D.M. terms' cumulative contribution is assumed to be negligible, far from acoustic's sources and axial boundaries of the wavetube. The time measurement of a sensor located at the same coordinate ($\boldsymbol{r}_s$) at time t_r is given by:

$$p_{s,r} = 2\mathrm{Re}\left(P_s e^{\mathrm{i}\omega t}\right) = \sum_\mu 2\mathrm{Re}\left(P_\mu^+\right)\cos\left(\omega t_r - k_\mu x_s\right) + 2\mathrm{Re}\left(P_\mu^-\right)\cos\left(\omega t_r + k_\mu x_s\right) -$$
$$2\mathrm{Im}\left(P_\mu^+\right)\sin\left(\omega t_r - k_\mu x_s\right) - 2\mathrm{Im}\left(P_\mu^-\right)\sin\left(\omega t_r + k_\mu x_s\right). \tag{4}$$

The real-value pressure function is used here since the identification procedure will be later implemented on a finite precision FPGA, and complex arithmetic cannot be used directly. By employing the sum of angles trigonometric identities, Eq. (4) can be written as:

$$p_{s,r} = \left(w_{\mu,1}\cos\left(k_\mu x_s\right) + w_{\mu,2}\sin\left(k_\mu x_s\right)\right)\cos(\omega t_r) + \left(w_{\mu,3}\cos\left(k_\mu x_s\right) + w_{\mu,4}\sin\left(k_\mu x_s\right)\right)\sin(\omega t_r), \quad (5)$$

where the relation between the real-valued wave coefficients vector $\mathbf{w}_\mu = \left[w_{\mu,1}, \dots, w_{\mu,4}\right]^T$ to the modal wave's complex amplitudes is given by:

$$\begin{bmatrix} P_\mu^+ \\ P_\mu^- \end{bmatrix} = \frac{1}{2J_{n_\mu}(\eta_\mu R)}\begin{bmatrix} 1 & \mathrm{i} & \mathrm{i} & -1 \\ 1 & -\mathrm{i} & \mathrm{i} & 1 \end{bmatrix}\boldsymbol{w}_\mu. \quad (6)$$

By defining

$$\mathbf{h}_\mu^{(s,r)} \equiv \left[\cos\left(k_\mu x_s\right)\cos(\omega t_r), \sin\left(k_\mu x\right)\cos(\omega t_r), \cos\left(k_\mu x_s\right)\sin(\omega t_r), \sin\left(k_\mu x_s\right)\sin(\omega t_r)\right]^T, \quad (7)$$

Equation (5), can be written as a vector product:

$$p_{s,r} = \sum_\mu \mathbf{h}_\mu^{(s,r)^T}\mathbf{w}_\mu = \mathbf{h}^{(s,r)^T}\mathbf{w}, \quad (8)$$

where $\mathbf{h}^{(s,r)} = \left[\mathbf{h}_1^{(s,r)^T}, \dots, \mathbf{h}_N^{(s,r)^T}\right]^T$, and $\mathbf{w} = [\mathbf{w}_1^T, \dots, \mathbf{w}_N^T]^T$.

B. Finite length wavetube and modal Traveling Wave Ratio

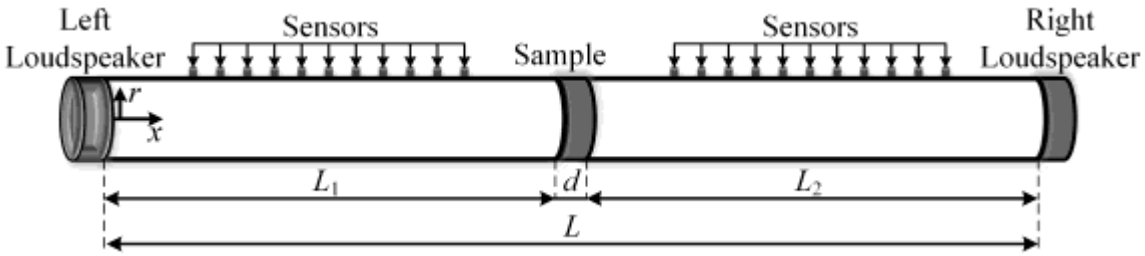

Fig 1. The wavetube model. L_1 and L_2 denote the length of the left side and right side of the tube accordingly. d represents the material's sample length and L the overall length of the tube. Two loudspeakers are placed at each tube's side, and sensors are placed along the tube axis at the outer diameter.

In this section, a finite-length elastic wavetube is considered. In the current derivation, the material sample is removed from the wavetube. The wavetube has a loudspeaker located at each end; it is assumed that there is no modal interaction at the boundaries and that the excitation forces are monochromatic. The boundary conditions under these assumptions can be written in their modal form as[7]:

$$\begin{bmatrix} 1+\frac{Z_{\mu,0}k_\mu}{\rho_f\omega} & 1-\frac{Z_{\mu,0}k_\mu}{\rho_f\omega} \\ \left(1-\frac{Z_{\mu,L}k_\mu}{\rho_f\omega}\right)e^{-ik_\mu L} & \left(1+\frac{Z_{\mu,L}k_\mu}{\rho_f\omega}\right)e^{ik_\mu L} \end{bmatrix} \begin{bmatrix} P_\mu^+ \\ P_\mu^- \end{bmatrix} = \begin{bmatrix} f_{\mu,0} \\ -f_{\mu,L} \end{bmatrix} \tag{9}$$

where $Z_{\mu,0}$ and $Z_{\mu,L}$ denote the loudspeakers' modal complex acoustic impedances, and $f_{\mu,0}$ and $f_{\mu,L}$ denotes modal forces that are obtained from the following projections:

$$f_{\mu,0} = \frac{1}{E_\mu^2}\int_0^R\int_0^{2\pi} e^{-in_\mu\theta}J_{n_\mu}(\eta_\mu r)F_{\text{spk},0}rdrd\theta\,, \quad f_{\mu,L} = \frac{1}{E_\mu^2}\int_0^R\int_0^{2\pi} e^{-in_\mu\theta}J_{n_\mu}(\eta_\mu r)F_{\text{spk,L}}rdrd\theta\,,$$

where $E_\mu^2 = 2\pi \int_0^b J_{n_\mu}^2(\eta_\mu r) r dr$ is the normalization factor of the propagation mode P_μ, and $F_{spk,0}$ and $F_{spk,L}$ are the loudspeakers' amplitudes.

Solving Eq. (9) gives the modal wave amplitudes subject to the projections of the excitation sources on the propagation mode

$$\begin{bmatrix} P_\mu^+ \\ -P_\mu^- \end{bmatrix} = \frac{1}{\Delta_\mu} \begin{bmatrix} \left(1 + \frac{Z_{\mu,L} k_\nu}{\rho_f \omega}\right) e^{ik_\mu L} f_{\mu,0} + \left(1 - \frac{Z_{\mu,0} k_\mu}{\rho_f \omega}\right) f_{\mu,L} \\ \left(1 - \frac{Z_{\mu,L} k_\nu}{\rho_f \omega}\right) e^{-ik_\mu L} f_{\mu,0} + \left(1 + \frac{Z_{\mu,0} k_\mu}{\rho_f \omega}\right) f_{\mu,L} \end{bmatrix}. \quad (10)$$

where Δ_μ denotes the matrix determinant of Eq. (9) left-hand-side matrix.

Having parametrized the multiple propagating waves, it is possible to compute the ratio of traveling to standing waves proportions for each wavelength associated with one modal component. This is done by computing the modal TWR that is defined as[11]:

$$\mathrm{TWR}_\mu \equiv 1 - \frac{\left||P_\mu^+| - |P_\mu^-|\right|}{|P_\mu^+| + |P_\mu^-|}. \quad (11)$$

The fraction represents the ratio between the traveling wave and the total wave amplitudes. The shifting is introduced to allow minimum seeking optimization technique for pure traveling wave control[38]. When the modal TWR is equal to zero ($\mathrm{TWR}_\mu = 0$) the mode is a pure traveling wave and when the modal TWR is equal to one ($\mathrm{TWR}_\mu = 1$) the mode is a pure standing wave. The modal traveling wave's direction of propagation denoted as dir_μ is defined by the sign of the numerator argument:

$$\mathrm{dir}_\mu \equiv \mathrm{sign}\left(|P_\mu^+| - |P_\mu^-|\right). \quad (12)$$

Substituting the modal forward and backward going traveling wave amplitudes obtained in Eq. (10) to Eq. (11) results in:

$$\mathrm{TWR}_{\mu} = 1 - \frac{\left|\left|v_{\mu,L}^{+} e^{\mathrm{i}k_{\mu}L} f_{\mu,0} + v_{\mu,0}^{-} f_{\mu,L}\right| - \left|v_{\mu,L}^{-} e^{-\mathrm{i}k_{\mu}L} f_{\mu,0} + v_{\mu,0}^{+} f_{\mu,L}\right|\right|}{\left|v_{\mu,L}^{+} e^{\mathrm{i}k_{\mu}L} f_{\mu,0} + v_{\mu,0}^{-} f_{\mu,L}\right| + \left|v_{\mu,L}^{-} e^{-\mathrm{i}k_{\mu}L} f_{\mu,0} + v_{\mu,0}^{+} f_{\mu,L}\right|}, \tag{13}$$

where $v_{\mu,0}^{\pm} = 1 \pm \mathrm{Z}_{\mu,0}\mathrm{k}_{\mu}/\rho_{\mathrm{f}}\omega$, and $v_{\mu,L}^{\pm} = 1 \pm \mathrm{Z}_{\mu,L}\mathrm{k}_{\mu}/\rho_{\mathrm{f}}\omega$ are the normalized modal loudspeakers' impedances. Writing the modal forces as $f_{\mu,0} = \left|f_{\mu,0}\right| e^{\mathrm{i}\varphi_0}$, and $f_{\mu,L} = \left|f_{\mu,L}\right| e^{\mathrm{i}\varphi_L}$, where φ_0, and φ_L are the same for all modes (this is seen from the projection integrals), and the normalized modal loudspeakers' impedances as $v_{\mu,0}^{\pm} = \left|v_{\mu,0}^{\pm}\right| e^{\mathrm{i}\phi_{\mu,0}}$ and $v_{\mu,L}^{\pm} = \left|v_{\mu,L}^{\pm}\right| e^{\mathrm{i}\phi_{\mu,L}}$ in Eq. (13) results in:

$$\mathrm{TWR}_{\mu} = 1 - \frac{\left|C_{\mu}\left|B_{\mu}^{+} e^{\mathrm{i}(k_{\mu}L + \Delta\phi^{+})} + A_r e^{\mathrm{i}\Delta\varphi}\right| - \left|B_{\mu}^{-} e^{-\mathrm{i}(k_{\mu}L + \Delta\phi^{-})} + A_r e^{\mathrm{i}\Delta\varphi}\right|\right|}{C_{\mu}\left|B_{\mu}^{+} e^{\mathrm{i}(k_{\mu}L + \Delta\phi^{+})} + A_r e^{\mathrm{i}\Delta\varphi}\right| + \left|B_{\mu}^{-} e^{-\mathrm{i}(k_{\mu}L + \Delta\phi^{-})} + A_r e^{\mathrm{i}\Delta\varphi}\right|}, \tag{14}$$

in which, $A_r \equiv \left|f_{\mu,L}\right| / \left|f_{\mu,0}\right|$ denotes the loudspeaker's amplitude ratio, $\Delta\varphi \equiv \varphi_L - \varphi_0$ the loudspeaker's phase shift, $B_{\mu}^{\pm} \equiv \left|v_{\mu,L}^{\pm}\right| / \left|v_{\mu,0}^{\mp}\right|$, $\Delta\phi_{\mu}^{\pm} = \pm\phi_{\mu,L}^{\pm} \mp \phi_{\mu,0}^{\mp}$, and $C_{\mu} \equiv \left|v_{\mu,0}^{-}\right| / \left|v_{\mu,0}^{+}\right|$. Equation. (14) portraits the surface of the modal traveling wave ratio as a function of the wavetube dispersion, the loudspeakers' acoustic impedances, and the amplitude ratio and phase shift between the loudspeakers. Therefore, if the modal TWR is to be set assuming that the different parameters of the model are known accurately, the nonlinear equation defined by Eq. (14) can be solved to find the required amplitude ratio and phase shift between the two loudspeakers.

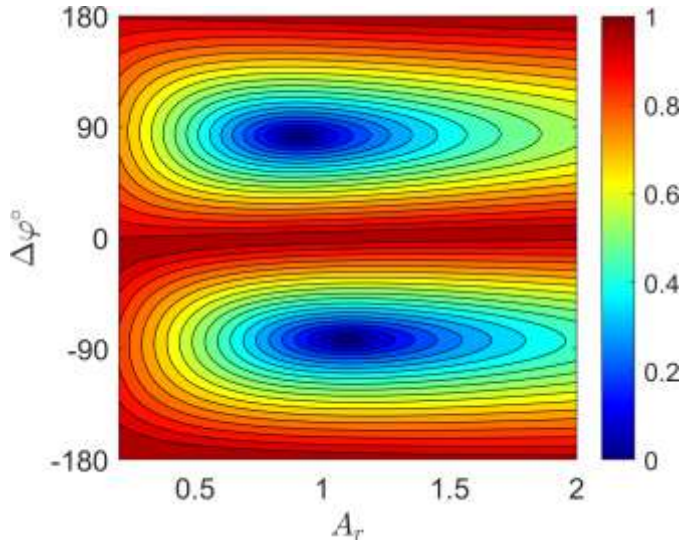

Fig 2. Analytical modeled modal traveling wave ratio, TWR_1, contour for a grid of loudspeaker's amplitude ratios and phase shifts based on the model of Eq. (14). The input parameters are: tube length $L = 2$ m, fluid sound speed $v_\mathrm{f} = 346$ m/sec, fluid density $\rho_\mathrm{f} = 1.2$ kg/m^3, angular frequency $\omega = 2\pi \cdot 1500$ rad/sec, modal wavenumber $k_1 = 27.2392$ rad/m, and loudspeaker's complex acoustic impedances $Z_{1,0} = Z_{1,L} = 1264.5e^{-\mathrm{i}\cdot 0.4488\pi}$ Pa/(m/sec).

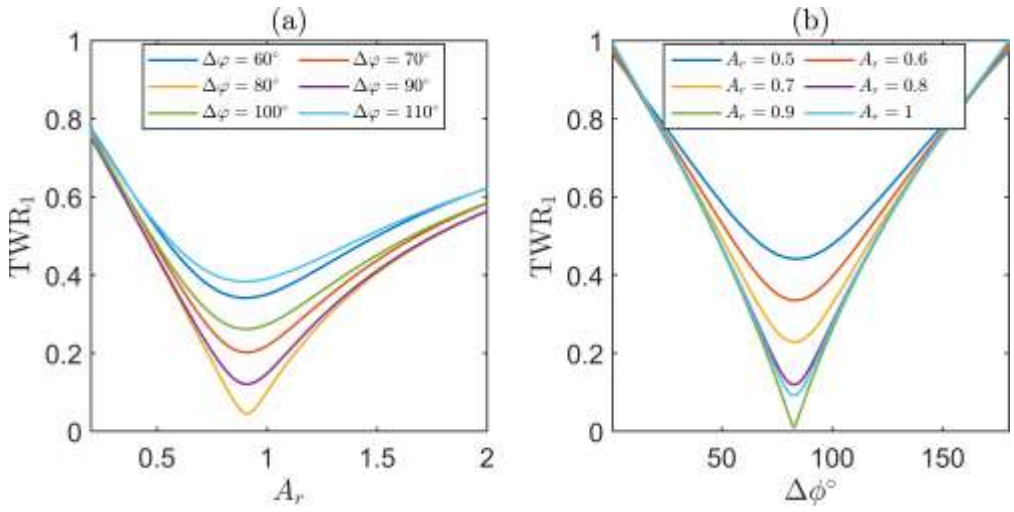

Fig 3. Slices from the analytical obtained modal traveling wave ratio contour shown in Fig 2. (a) – Equal phase shifts contours. (b) – Equal amplitude ratio contours.

The modal TWR of the first acoustic mode is shown in Fig 2 for a grid of loudspeaker amplitude ratios and phase shifts for prechosen values of the other model parameters. The dark red regions are pure standing wave regions, while the blue regions represent the pure traveling wave regions. The upper half of the TWR contour ($\Delta\varphi \geq 0$) corresponds to forward traveling waves (dir_1=1), and the lower half ($\Delta\varphi < 0$) corresponds to backward traveling waves (dir_1 =–1). Note that both slices at constant phase shift and slices at constant amplitude ratio are convex functions, as is seen from the contours of Fig 3. It is also shown in Fig 2 and Fig 3(b) that the mapping between the loudspeaker's amplitude ratio and phase shift to the modal traveling wave ratio is surjective; therefore, these parameters may be tuned to excite any desirable value of the modal traveling wave ratio.

As discussed from and analytically viewpoint[14] and shown experimentally for the air-filled impedance-tube[38], the values of to be tuned loudspeaker's parameters, A_r and $\Delta\varphi$, have high sensitivity with respect to the model parameters accuracy. Therefore, an online update procedure is required. Since the mapping from the loudspeaker's parameters to the modal traveling wave ratio is both surjective and convex, a model-based, gradient-descend adaptive control schematic is put forward.

III. CONTROL AND ESTIMATION FORMULATION

In this section, the adaptive control algorithm is developed for an air-filled elastic impedance tube. The derivation is based on the mathematical formulation presented in section II. It is assumed that the coupling between the fluid and the elastic tube is strong enough to excite multiple modes at all frequencies, each with a different amplitude. In the current work, only the first axisymmetric acoustic mode, with the modal order $(n, m) = (0,1)$, is being controlled. It was

shown[11] that in order to fit an accurate model for the $(0,1)$ propagation mode using a least-squares approach, additional modes must be included in the pressure model as well. Specifically, the second acoustic mode $(0,2)$ and the first flexural mode $(\pm 1,1)$.

The control adaptation law is derived based on the analytical model of the modal traveling wave ratio introduced in Section II. A closed domain of the control parameter is chosen to ensure stability. The periodic extension of the closed domain is achieved using modulo arithmetic. Three methods are described and compared to estimate the TWR gradient.

To enable the real-time estimation of the traveling wave ratio, which is needed for the control law, a multichannel LMS algorithm is proposed. The LMS fits the real-valued modal amplitudes introduced in Section II (Eq. (8)) using the matrix **h** as the filter matrix. The dispersion model was calibrated to match the experimental system in a previous work[6]. When applied to the air-filled impedance tube, the LMS convergence and attributes were discussed previously[11].

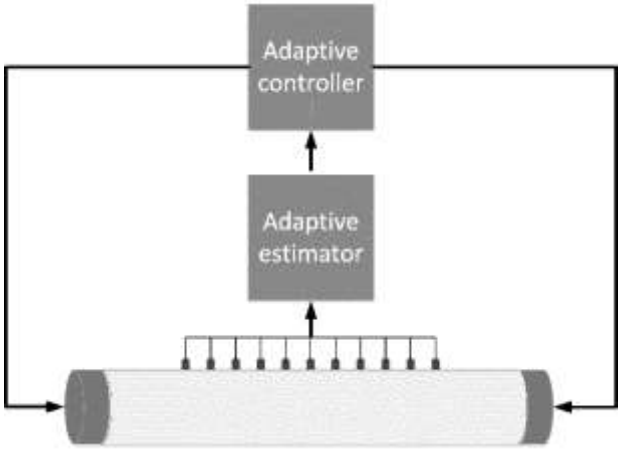

Fig 4. Adaptive control and experimental system setup description. Microphones' outputs are measured and decomposed into their propagating wave's modal amplitudes using an adaptive estimator. The modal amplitudes are sent to the adaptive control law that controls the loudspeaker's amplitude ratio and phase shift to track the reference modal TWR signal.

A. ADAPTIVE CONTROL-LAW DERIVATION

Following the discussion of Section II.B, it is concluded that there are two local minima of the TWR that correspond to the pure forward and backward going traveling waves. When examining Fig 2, a clear separation between the forward and backward traveling wave region is evident; this can be rigorously justified by finding the zeros of the modal direction of Eq. (12), which can be written for the case of $Z_{1,0} = Z_{1,L}$ as:

$$\mathrm{dir}_{\mu} = 0 \rightarrow \sin(\Delta\varphi) = \frac{A_r - A_r^{-1}}{4\sin\left(k_{\mu}L + \Delta\phi^{+}\right)}\left(\left|\frac{\upsilon_{\mu}^{+}}{\upsilon_{\mu}^{-}}\right| - \left|\frac{\upsilon_{\mu}^{-}}{\upsilon_{\mu}^{+}}\right|\right), \tag{15}$$

Where $\upsilon_{\mu,0}^{\pm} = \upsilon_{\mu,L}^{\pm} = \upsilon_{\mu}^{\pm}$. If the ratio $\left|\upsilon_{\mu}^{+}/\upsilon_{\mu}^{-}\right|$ is close to unity, which is our case, then the direction is switched at $1 \gg \Delta\varphi > 0$, which is justified by the TWR contour plotted for 1500 Hz. The direction is correlated with the sign of the phase shift, forward for positive and backward for negative. Therefore, the control law is developed for phase shift bounded between 0º to 180º. If backward traveling waves are desired, the phase shift's output signal will be multiplied by –1. Therefore it is assumed that the traveling wave is a forward going one and the absolute value of the numerator of Eq. (14) is discarded, which simplifies to:

$$\mathrm{TWR}_{\mu}^{+} = \frac{2\sqrt{B_{\mu}^{-2} + A_r^2 + 2B_{\mu}^{-}A_r\cos\left(k_{\mu}L + \Delta\phi^{+} + \Delta\varphi\right)}}{C_{\mu}\sqrt{B_{\mu}^{+2} + A_r^2 + 2B_{\mu}^{+}A_r\cos\left(k_{\mu}L + \Delta\phi^{+} - \Delta\varphi\right)} + \sqrt{B_{\mu}^{-2} + A_r^2 + 2B_{\mu}^{-}A_r\cos\left(k_{\mu}L + \Delta\phi^{-} + \Delta\varphi\right)}}$$

(16)

In Eq. (16) , superscript + of the TWR denote that this is the case of a forward-going traveling wave.

The control goal is to enable the tracking of a desired $\mathrm{TWR}_{\mathrm{ref}}$. Defining the tracking error:

$$e_{\mu}(\chi)=\mathrm{TWR}_{ref}-\mathrm{TWR}_{\mu}(\chi) \tag{17}$$

where $\chi=[A_r,\Delta\varphi]^T$ denotes the controlled parameter vector. The control goal is obtainable by minimizing the tracking error energy,e_{μ}^2, using a gradient descent formulism[43,44]:

$$\chi^{(r+1)}=\chi^{(r)}-\mathbf{K}\left(\nabla_{\chi}e_{\mu}^2\right)_{\chi=\chi^{(r)}}=\chi^{(r)}+2e_{\mu}^{(r)}\mathbf{K}\left(\nabla_{\chi}\mathrm{TWR}_{\mu}\right)_{\chi=\chi^{(r)}}. \tag{18}$$

where superscript (r) denotes the r^{th} iteration instance and the matrix $\mathbf{K}\in\mathbb{R}^{2\times2}$ is the adaptation gain matrix. In the general case, **K** can be regarded as a full matrix. In this work, it is assumed that the matrix is diagonal. Meaning that the control law can be implemented separately for each of the control parameters. In this case, Eq. (18) can be written as:

$$A_r^{(r+1)}=A_r^{(r)}+\kappa_{A_r}e_{\mu}^{(r)}\frac{\partial\mathrm{TWR}_{\mu}^{(r)}}{\partial A_r},\quad \Delta\varphi_r^{(r+1)}=\Delta\varphi_r^{(r)}+\kappa_{\Delta\varphi}e_{\mu}^{(r)}\frac{\partial\mathrm{TWR}_{\mu}^{(r)}}{\partial\Delta\varphi}, \tag{19}$$

where κ_{A_r} and $\kappa_{\Delta\varphi}$ are the scalar adaptation gains. The derivative of the modal traveling wave ratio, TWR_{μ}, with respect to the loudspeakers' amplitude ratio and phase shift can be computed from the analytical model based on Eq. (16). Since the uncertainties in the model parameters will affect the TWR derivatives as well, instead of using the exact derivatives, several approximations are considered.

To guarantee the stability of all approximations and ensure that the loudspeaker amplitude will not diverge rapidly, a periodic extension of the control parameters is suggested. The extension is made plausible since, as is seen in Fig 2, the TWR is a surjective mapping, i.e., TWR$\in(0,1)$, inside the bounded squared parameter domain $A_r\in(0.5,2)\times\Delta\varphi\in(0,\pi)$. Thus, a periodic extension of the parameter's region is available by the introduction of a shift operator and modulo arithmetic:

$$A_r = 0.5 + \Delta A_r, \quad \Delta A_r = \mathrm{mod}\left(\Delta A_r, 1.5\right), \quad \Delta\varphi = \mathrm{mod}\left(\Delta\varphi, \pi\right). \tag{20}$$

By introducing the periodic extension of the controlled parameters, the adaptation law stability is guaranteed. Only the convergence of the chosen law should be considered by tuning the adaptation gains and adaptation times (which may differ). The adaptation-laws of Eq. (19) remains the same under the periodic extension of Eq. (20), with the only change being $A_r \rightarrow \Delta A_r$:

$$\Delta A_r^{(r+1)} = \Delta A_r^{(r)} + \kappa_{A_r} e_\mu^{(r)} \frac{\partial \mathrm{TWR}_\mu^{(r)}}{\partial A_r}. \tag{21}$$

When backward going waves are required, the almost symmetrical behavior when changing roles between the reference and controlled loudspeakers (for similar loudspeakers, $Z_0 \cong Z_L$), is utilized. The output phase shift of the adaptation law is negated by multiplying: $\Delta\varphi_{out} = \Delta\varphi \cdot \mathrm{dir}_{ref}$; and the amplitude ratio is inverted around the $A_r = 1$ axis by taking the power $A_{r,out} = A_r^{\mathrm{dir}_{ref}}$, before feeding them to the system. Doing so will ensure that the obtained TWR will be similar to that of the forward traveling wave before the inversion and phase shifting.

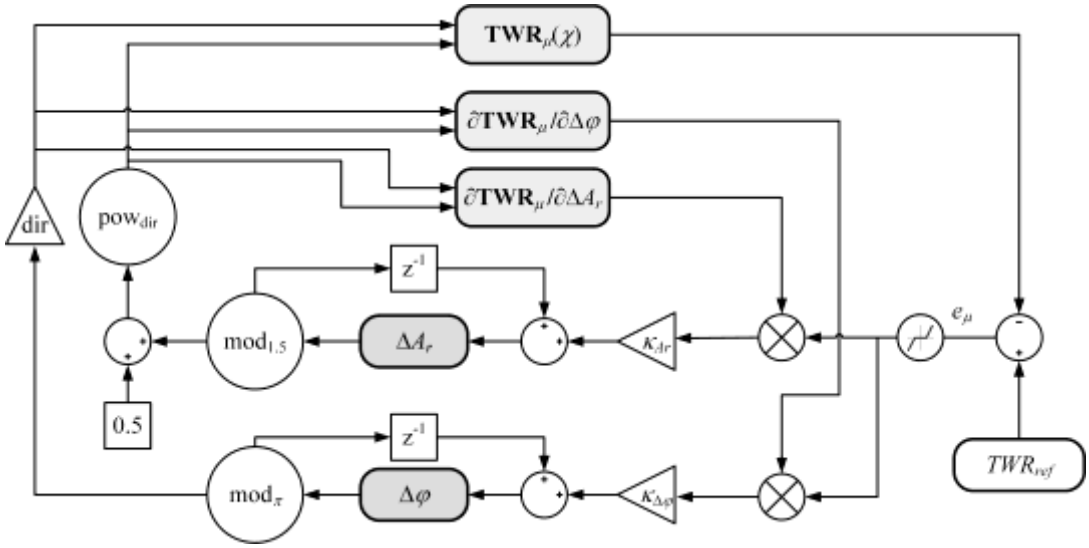

Fig 5. Adaptation-law block diagram. × denotes multiplication, mod_x denotes the modulo x function, pow_x denotes the input power to the x, dir is the required reference direction of propagation, and z^{-1} denotes the unit-step delay element. The TWR block represents the mapping between the loudspeaker's amplitude ratio and phase shift to the modal traveling wave ratio.

The adaptation law is presented in Fig 5, where the gradient approximation sub-system in this work is considered either one of the three possibilities discussed in the following sub-sections: the finite-difference, the extremum seeking, and the zero-order approximations.

1. *Finite-difference approximation*

The finite-difference approximation assumes that the two control parameters mutual effect is negligible. Therefore, the derivative with respect to each of the parameters may be written using a backward finite difference as:

$$\frac{\partial \text{TWR}_\mu^{(r)}}{\partial \xi} \approx \text{sign}\left(\xi^{(r)} - \xi^{(r-1)}\right) \frac{\text{TWR}_\mu^{(r)} - \text{TWR}_\mu^{(r-1)}}{\left|\xi^{(r)} - \xi^{(r-1)}\right| + \varepsilon} + a\,, \tag{22}$$

where ξ denote the control parameter, either A_r or $\Delta\varphi$, $0 < \varepsilon \ll 1$ is introduced to ensure numerical stability and is chosen to be around the machine precision, and $a \ll 1$ is used to jumpstart and avoid undesired local roots of the gradient surface. The approximated derivative is passed via a saturation function to maintain reasonable smoothness similar to the one observed in Fig 2.

2. *Extremum seeking*

By modulating each control parameter with a small amplitude oscillation around its nominal value, one may write the TWR as:

$$\mathrm{TWR}\left(A_r + a_1 \sin\omega_1 t, \Delta\varphi + a_2 \sin\omega_2 t\right). \tag{23}$$

Since the input is periodic, one may expand the TWR using its Fourier series:

$$\mathrm{TWR} = \mathrm{TWR}_0 + \sum_{n=1}^{\infty} a_{s,n} \sin n\omega_1 t + a_{c,n} \cos n\omega_1 t + \sum_{m=1}^{\infty} b_{s,m} \sin m\omega_2 t + b_{c,m} \cos m\omega_2 t\,. \tag{24}$$

The constant TWR_0 is removed by passing the measured TWR via a high-pass filter (HPF). Then, by multiplying the results with the modulation function $2\sin\omega_1 t$, and passing it via a low-pass filter (LPF) results in

$$2\mathrm{LPF}\left[\sin\omega_1 t \cdot \mathrm{HPF}[\mathrm{TWR}]\right] = \mathrm{LPF}\left[\begin{array}{l} \sum_{n=1}^{\infty} a_{s,n}\left(\cos(n-1)\omega_1 t - \cos(n+1)\omega_1 t\right) \\ +a_{c,n}\left(\sin(n+1)\omega_1 t - \sin(n-1)\omega_1 t\right) \\ +\sum_{m=1}^{\infty} b_{s,m}\left(\cos\left(m\omega_2 - \omega_1\right)t - \cos\left(\omega_1 + m\omega_2\right)t\right) \\ +b_{c,m}\left(\sin\left(\omega_1 + m\omega_2\right)t - \sin\left(m\omega_2 - \omega_1\right)t\right) \end{array}\right] = a_{s,1}, \tag{25}$$

where the last equality is valid as long as the LPF bandpass is set lower $\min_{m=0,1,\ldots} |m\omega_2 - \omega_1|$. Similarly, one may extract $b_{s,1}$ by multiplying with the second modulation function $2\sin\omega_2 t$. In

addition, considering the Taylor expansion of the TWR with respect to the two parameters, it follows:

$$\mathrm{TWR}\left(A_r + a_1 \sin\omega_1 t, \Delta\varphi + a_2 \sin\omega_2 t\right) \approx \mathrm{TWR}\left(A_r, \Delta\varphi\right) + \frac{\partial \mathrm{TWR}}{A_r} a_1 \sin\omega_1 t + \frac{\partial \mathrm{TWR}}{\Delta\varphi} a_2 \sin\omega_2 t + \cdots \tag{26}$$

By equating Eq. (25) and (26), it follows that

$$\begin{aligned} \frac{\partial \mathrm{TWR}}{A_r} a_1 &\approx a_{s,1} = 2\mathrm{LPF}\left[\sin\omega_1 \mathrm{t} \cdot \mathrm{HPF}[\mathrm{TWR}]\right] \\ \frac{\partial \mathrm{TWR}}{\Delta\varphi} a_2 &\approx b_{s,1} = 2\mathrm{LPF}\left[\sin\omega_2 \mathrm{t} \cdot \mathrm{HPF}[\mathrm{TWR}]\right] \end{aligned}, \tag{27}$$

which is visualized by the block diagram given in Fig 6.

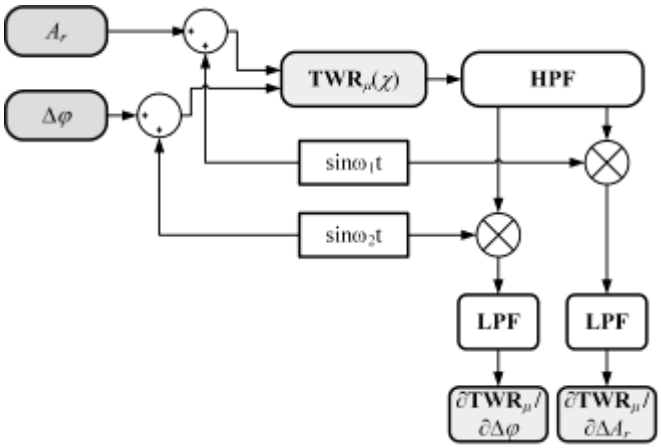

Fig 6. Extremum seeking approximation for partial derivatives of the TWR with respect to the control parameters.

Therefore, by introducing the modulation function and the described signal processing, the partial derivatives of the modal traveling wave are approximated.

3. *Zero-order approximation*

From the definition of the traveling wave ratio, an intrinsic property is that its derivative at TWR=0 is zero. By deriving the series approximation of the TWR around $\mathrm{TWR} = 0$ and assuming a lossless and delay-free system, meaning the pure traveling wave are obtained at $A_r = 1$, and $\Delta\varphi = -kL$. The linear approximations of the derivatives under these assumptions are

$$\frac{\partial \mathrm{TWR}_{\mu}^{(r)}}{\partial A_r} \approx C_1 \mathrm{TWR}_{\mu}^{(r)} \quad \frac{\partial \mathrm{TWR}_{\mu}^{(r)}}{\partial \Delta\varphi} \approx C_2 \mathrm{TWR}_{\mu}^{(r)} \tag{28}$$

where C_1 and C_2 depends on the loudspeaker's properties, the tube length, and the modal wavenumber, which are constant with respect to the adaptation law. Note that by taking the zero-order approximation, the TWR derivatives have a constant sign. The convergence, in this case, is made plausible due to the periodic extension of the control parameter's region. This feature of the adaptation law will be discussed based on the numerical simulation results presented in the next section.

4. *Simulation result*

Using the TWR expression given in Eq. (14), and based on the adaptive control law block diagram of Fig 5, a Simulink© simulation was created to validate the control law and find an initial guess to the adaptation gains ($\kappa's$). The simulation was done in discrete timesteps. The reference TWR was changed every 1000 steps, the reference propagation direction was changed every 10000 steps, and the error dead-zone was set to ± 0.002. The amplitude ratio adaptation gain was set to $\kappa_{A_r} = 0.5$, and the phase shift adaptation gain to $\kappa_{\Delta\varphi} = 0.1$. Initial values were taken for the case of perfect wavetube and pure traveling wave, for which the loudspeakers are lossless, meaning that $A_r = 1 \rightarrow \Delta A_r^{(0)} = 0.5$, and to match the propagation phase the phase shift is

$\Delta\varphi^{(0)} = \omega L/c_{\mathrm{f}}$. For the Extremum seeking the modulation frequencies were chosen to be $\omega_1 = 2\pi/30$ (rad/sample), and $\omega_2 = 2\pi/25$ (rad/sample) respectively, the HPF was done using the Simulink's© DC Blocker, and the LPF was realized using resettable integral filter, which was initialized at each change of the reference TWR.

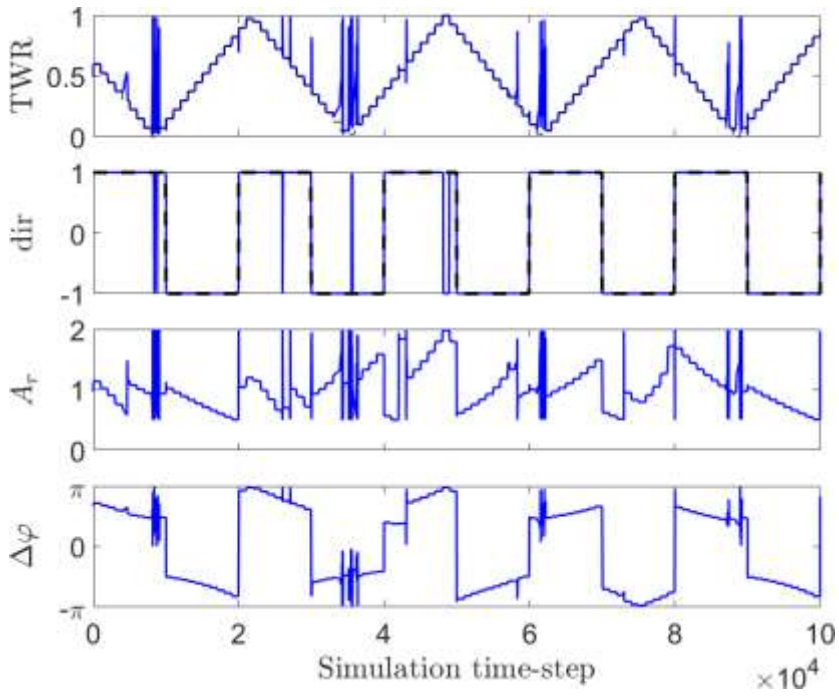

Fig 7. Simulation results of the proposed adaptive control when the TWR gradient is estimated via the finite difference approximation. Dashed line (black) – Reference TWR and dir. Solid line (blue) – Simulation outputs.

The simulation results when the TWR gradient is estimated using the finite difference approximation are shown in Fig 7. It is noted that for most reference TWR, the control algorithm converges in a reasonable number of steps. Moreover, when the dir reference is changed, convergence is almost immediately. Finally, when the reference TWR is small, convergence is not guaranteed. The latter can be improved by decreasing the adaptation gains' values at the trade-off

of slower convergence. The analysis and simulation shown here are for perfect measurements, i.e., no noise is added. The finite derivative approximation is highly sensitive when considerable measurement noise is present.

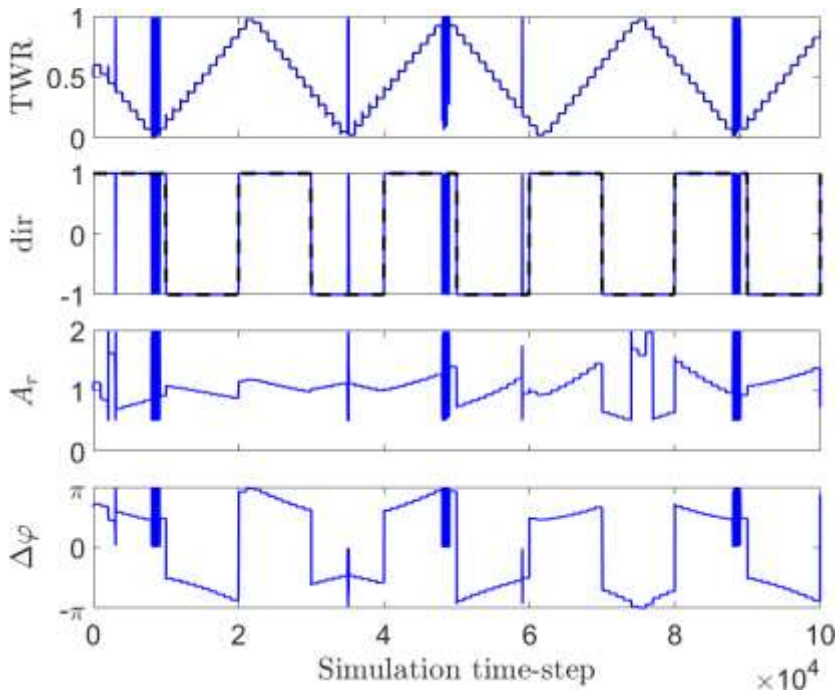

Fig 8. Simulation results of the proposed adaptive control when the TWR gradient is estimated using the Extremum seeking. Dashed line (black) – Reference TWR and dir. Solid line (blue) – Simulation outputs.

The simulation results when the TWR gradient is estimated via the extremum seeking algorithm are shown in Fig 8. It is noted that the convergence time and the control parameters' smoothness are better than those obtained using the finite derivative approximation (Fig 7). When the reference TWR is either near zero or one, the TWR does not necessarily converge. However, it can be seen that for half of these cases, the control has converged to the desired TWR. Unlike

the finite difference approximation, the Extremum seeking implementation is not straightforward. There is a need to tune the modulation frequencies, design and implement the HPF and LPF and ensure their convergence. Suppose some of the system parameters will change over time. In that case, it is not guaranteed that the initial controller design will be robust.

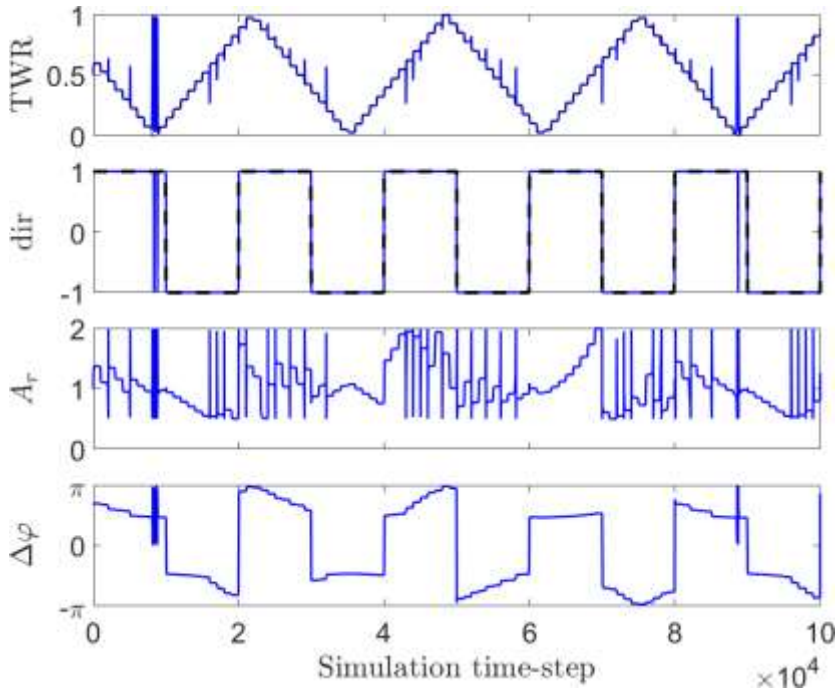

Fig 9. Simulation results of the proposed adaptive control when the TWR gradient is estimated via the zero-order approximation. Dashed line (black) – Reference TWR and dir. Solid line (blue) – Simulation outputs.

The simulation results when the TWR gradient was estimated via the zero-order approximation are shown in Fig 9. It is noted that convergence time is comparable with that of the Extremum seeking. The obtained amplitude ratio is more oscillatory than the one obtained from the Extremum seeking. This is since the gradient sign is constant. However, the phase shift seems to behave similarly. The control, in this case, was able to converge to all the desired

reference values, even for values near zero or one. The advantage of the zero-order approximation over the Extremum seeking is that there is no need to design any additional filters. When compared to the finite difference approximation, the zero-order approximation performance is better. Moreover, the adaptation for the zero-order approximation is memoryless, rendering it less sensitive to measurement noise.

Based on these results, it was decided to use the zero-order approximation to estimate the TWR gradient. The adaptive feedforward block diagram for this case is shown in Fig 10. In the next section, the adaptive estimation of the TWR from the pressure measurements will be portrait.

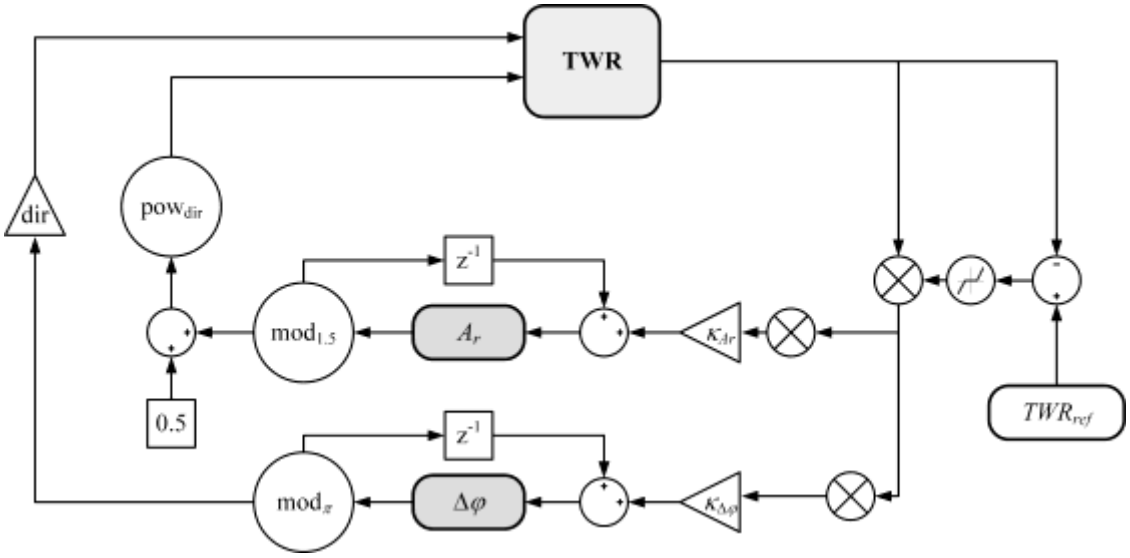

Fig 10. Adaptive control-law block diagram based on the zero-order approximation of the TWR gradient. × denotes multiplication, mod_x denotes the modulo x function, pow_x denotes the input power to the x, the ± is chosen by the desired direction, and z^{-1} denotes the unit delay element. The TWR is being estimated adaptively using the MC-LMS algorithm described in Section III.B.

B. ADAPTIVE ESTIMATION – MULTICHANNEL LEAST-MEAN-SQUARES MODEL

Since the traveling wave ratio, which is the input to the adaptation law, is not a measurable signal, an adaptive estimation is used. In previous work[11], different algorithms for the recursive real-time identification of **w** where discussed. It has been concluded that the MC-LMS[39] has the advantage of ease-of-implementation over the longer convergence-time when compared to the other recursive methods in the presence of measurement noise. Therefore, the MC-LMS was employed in the current effort to control the TWR as the wave decomposition algorithm. The MC-LMS is implemented on the FPGA using the block diagram presented in Fig 11. Note that only multiplications and additions are needed to execute the recursive law; this is the LMS method's main advantage.

The modal wavenumbers (k_μ) and their modal phase velocities ($c_{p,\mu}=\omega/k_\mu$) of the air-filled impedance tube used in this experimental setup (shown in Fig 14 in the Appendix), were identified previously[6] using the two-actuators phase-perturbations method as a function of the excitation frequency. The identified dispersion relation is shown in Fig 12; note that five modes were identified at the frequency band of interest. Out of the five modes, three were included in the reduced-order model, based on the result of a model-order L-curve regularization test[11] done on the air-filled tube. The modes used in the current identification procedure are the first ($n = 0, m = 1$) and second ($n = 0, m = 2$) axisymmetric modes, and the first flexural ($n = \pm 1, m = 1$) mode.

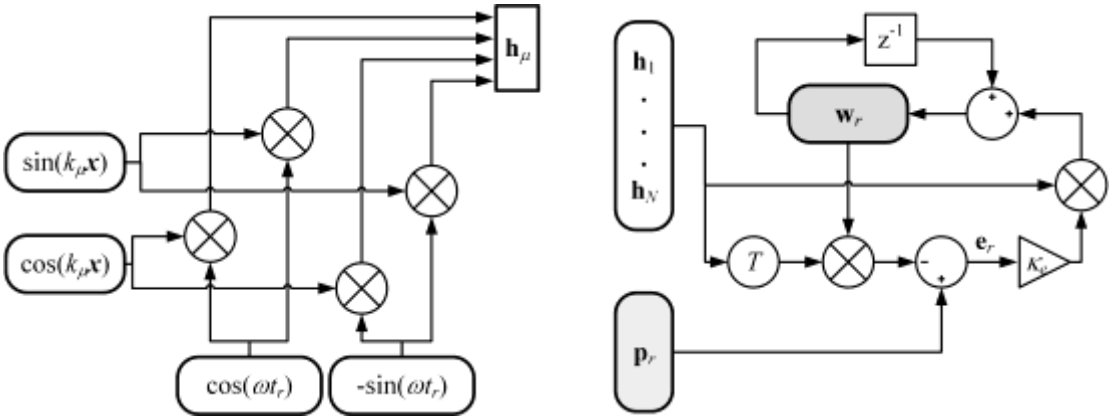

Fig 11. MC-LMS block-diagram, k_μ denotes the modal wavenumbers, ω the excitation frequency, $\boldsymbol{x}$ the microphone axial location vector, $t_r = rt_s$ stands for the r^{th} sampled time, $\mathbf{p}_r$ is the measured pressure vector at time t_r, $\mathbf{h}_\mu$ is the vector function defined in Eq. (7). $\times$ and T denote the vector multiplication and real transpose operators, respectively. z^{-1} denotes the unit-delay element, κ_e is the adaptive estimation gain coefficient, $\mathbf{e}_r$ the estimated error vector, and $\mathbf{w}_r^T = [\mathbf{w}_1^T \quad \cdots \quad \mathbf{w}_N^T]$ is the weight vector at the sampled time t_r.

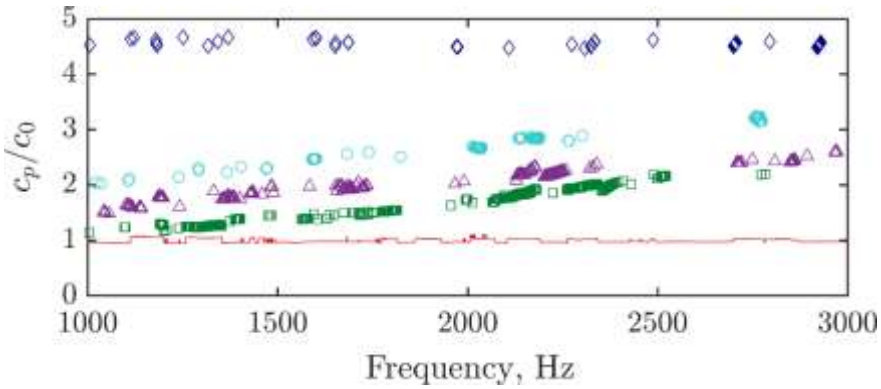

Fig 12. Identified dispersion curves of the PMMA air-filled impedance tube using the two-actuator phase-perturbations method, c_0 denotes the intrinsic speed of sound in air. Legend: solid line (red) – first axisymmetric mode; diamond markers (blue)– second

axisymmetric mode; square markers (green), circle markers (teal), and triangular markers (purple) – flexural modes.

Using the previously introduced MC-LMS method on the impedance tube (shown in Fig 14 in the Appendix), the TWR_n of all dominant modes were identified for a prescribed grid of amplitude gains (A_r) and phase shifts ($\Delta\varphi$) at an excitation frequency of 1500 Hz. The first axisymmetric mode's identified TWR_1 contour is shown in Fig 13.

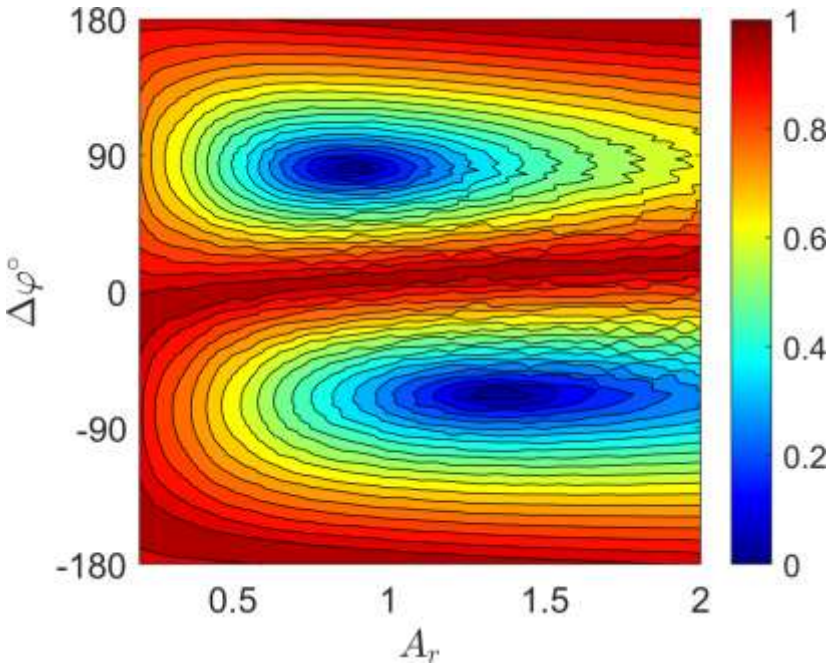

Fig 13. Identified TWR_1 contour plot. Obtained from the experimentally measured data for a prescribed grid of amplitude ratios (A_r) and phase shifts ($\Delta\varphi$) applied to the air-filled impedance tube. Identified from the MC-LMS method at an excitation frequency of 1500 Hz.

Note that the experimentally identified contour of Fig 13 is similar to that of the analytical model (Fig 2), even though not all of the system's dynamic was modeled.

Since the TWR is a steady-state phenomenon, the closed-loop control sample rate is reduced to be of a similar order to that of the steady-state convergence-time of the TWR, which was identified experimentally to be about 0.2 seconds at 1500 Hz. The two decoupled closed-loop control block diagrams are depicted in Fig 10.

IV. EXPERIMENTAL RESULTS AND DISCUSSION

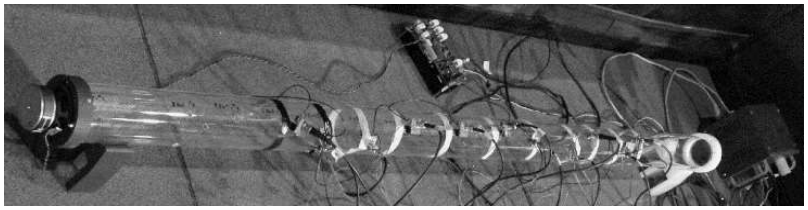

Fig 14. A photograph of the air-filled impedance tube was used in the experiment study case.

A photo of the system used for the experimental study of the suggested control schematic is shown in Fig. 14. An air-filled thin plastic (PMMA) tube of a circular cross-section was used as the waveguide under investigation. Two 3", 4 Ω, and 60 W Dayton Audio© PC83-4 loudspeakers are connected on each tube's ends. Eleven 9.7 mm diameter omnidirectional Adafruit© Max9814 microphones are located along the tube axis. The microphones are placed at the tube's inner diameter at a constant azimuthal angle. The signal-processing flow diagram used to implement the control schematic presented in Fig 10 is shown in Fig 15.

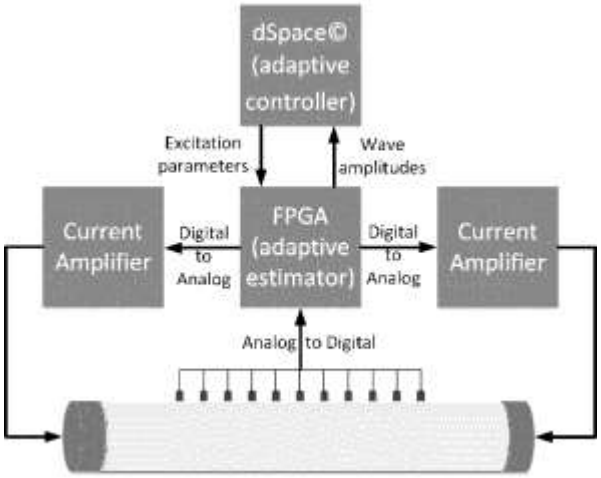

Fig 15. The flow diagram of the signal-processing layout.

The measurements are conducted using two DS5203 FPGA boards with sixteen 10 MHz and 15 bits analog to digital converter channels. The adaptive estimation used for the wave decomposition is implemented on the FPGA and runs at a fast rate. The estimated waves' modal amplitudes are transmitted to the dSPACE© DS1005 computational node with a sampling frequency of 1000 Hz and 32 bits communication channels. The modal TWR computation and the adaptive control-law are implemented using the DS1005 computation node, which sends the required loudspeakers amplitude ratio and phase shift to the FPGA. The loudspeakers are driven using two 10 MHz and 15 bits digital to analog channels of the FPGA and two analog current amplifiers introduced to eliminate the loudspeaker electrical impedance coupling the acoustic field.

The MC-LMS adaptive estimation algorithm was implemented on the DS5203 FPGA at 0.5 MHz sample frequency. The identified weight vector of Eq. (13). is transmitted to the DS1005 computation node controller. The suggested adaptive control law was implemented on the DS1005 at a 2 Hz sample frequency. Both the control parameters A_r and $\Delta\varphi$ are transmitted back to the

FPGA. The two loudspeaker excitation signals are generated by the FPGA and are transmitted via the current amplifiers.

The first set of experiments introduced a reference signal composed of several different constant values of the TWR_{ref} at excitation frequency 1500 Hz. This frequency was used to identify the TWR_1 contour shown in Fig 16, and on its basis, the control law was developed. The adaptive control reference tracking result is shown in Fig 16. The microphones measured signals and complex amplitude with and without modal decomposition are presented in Fig 17.

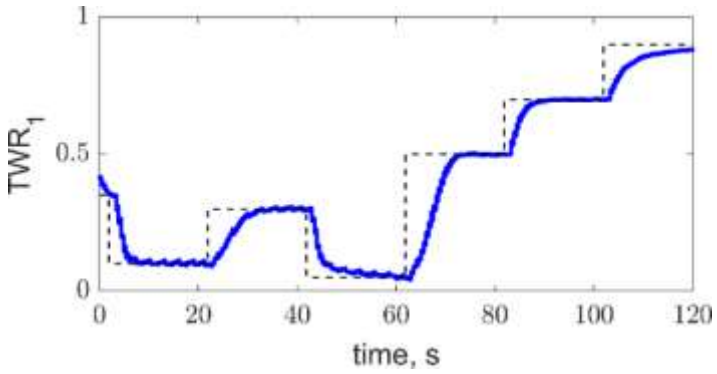

Fig 16. Measured TWR_1 from the adaptive control reference tracking experiment at an excitation frequency of 1500 Hz. Solid line – Measured TWR_1. Dashed line – Reference TWR_1.

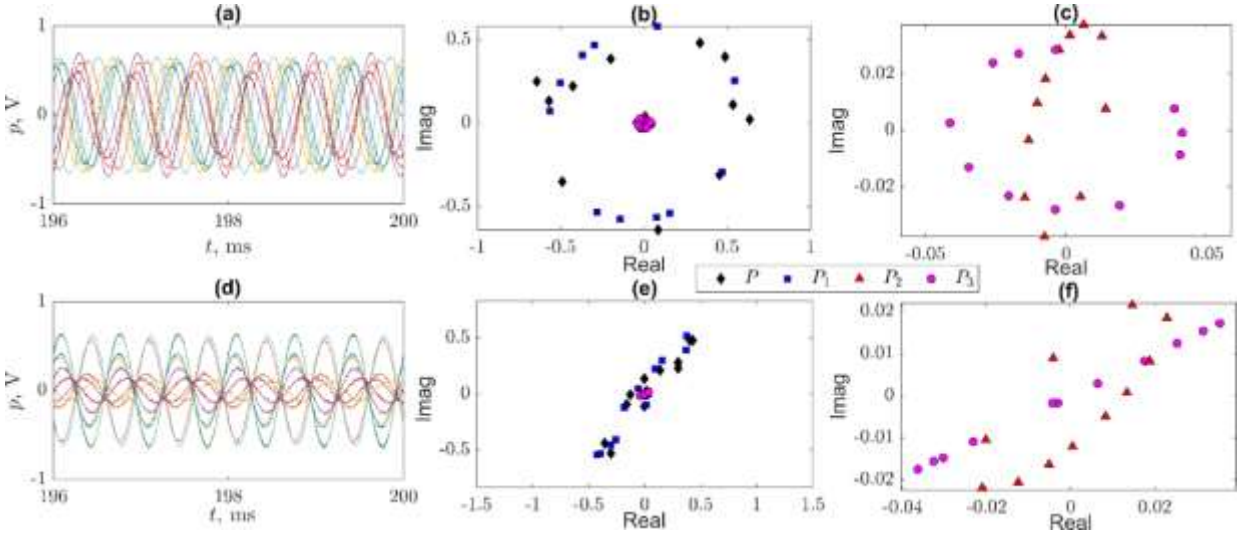

Fig 17. Measured adaptive control reference tracking at an excitation frequency of 1500 Hz. (a) – Microphones' measured signal at TWR_{ref}=0.1. (b) – Microphones' complex amplitudes and complex modal amplitudes at TWR_{ref}=0.1. (c) – Second and Third modes complex amplitudes at TWR_{ref}=0.1.

(d) – Microphones' measured signal at TWR_{ref}=0.9. (e) – Microphones' complex amplitudes and complex modal amplitudes at TWR_{ref}=0.9. (f) – Second and Third modes complex amplitudes at TWR_{ref}=0.9.

The reference tracking result presented in Fig 16 demonstrates the suggested method's capability to successfully manipulate the modal wave as desired by achieving the required modal TWR. The time-series measurements at steady state for TWR_{ref}=0.1 and TWR_{ref}=0.9 are presented in Fig 17(a) and Fig 17(d). Fig 17(a) shows that all microphone signals have similar amplitudes and that their phases differ proportionally to their location, suggesting that the waves are of a traveling nature. Contrary, in Fig 17(d), the microphone signals are in similar phases, and that their amplitudes differ, suggesting that the waves are almost of pure standing nature.

The same behavior can be analyzed by inspecting the microphone complex amplitudes, as shown in Fig 17(b) and Fig 17(e). The black diamond markers stand for the complex amplitudes of each microphone. By looking at the geometric structure, it can be seen that in Fig 17(b), the complex amplitudes form a circle-like shape, which suggests that the waves are of a more traveling nature; moreover, the complex amplitudes of Fig 17(e) take the form of a cigar-like ellipse indicating that the waves are of more standing nature. A more profound understanding of the wave's nature is made by inspecting each mode's complex amplitudes shown in Fig 17(b) and Fig 17(e) in the blue square, red triangle, and magenta circle markers for the first, second, and

third modes, respectively. In the case where the control reference was set to TWR_{ref}=0.1, the first mode's complex amplitude forms a circle-like shape, which indicates its traveling wave nature[13]. Moreover, both the second and third complex modal amplitudes (Fig 17(c)) form ellipses suggesting their mixed traveling and standing waves. By inspecting the two ellipses, it is concluded that the second mode is of a more standing-wave nature while the third mode is of a more traveling-wave nature.

Similar observations can be made for the case where the control reference was set to TWR_{ref}=0.9. The first mode complex amplitudes form a cigar-like ellipse, which indicates its standing-wave nature. Moreover, in this case, the third mode complex amplitudes (Fig 17(e) magenta circle markers) form a straight line suggesting an almost pure-standing wave. In contrast, the second mode complex amplitudes (Fig 17 (e) red triangle markers) form a cigar-like ellipse indicating a mixture of traveling-standing-waves where the standing wave is dominant. These observations can be quantified using the modal TWR, computed based on each ellipse curve fitting[13].

The results presented in Fig 16 and Fig 17 verify the assumptions used during the control's development at the 1500 Hz excitation frequency. To ensure that the assumptions held at different frequencies, a similar set of reference step tracking experiments were repeated at the excitation frequencies of 1000, 2000, 2500, and 3000 Hz. The modal wavenumbers were updated at each frequency according to the identified dispersion relation presented in Fig 12.

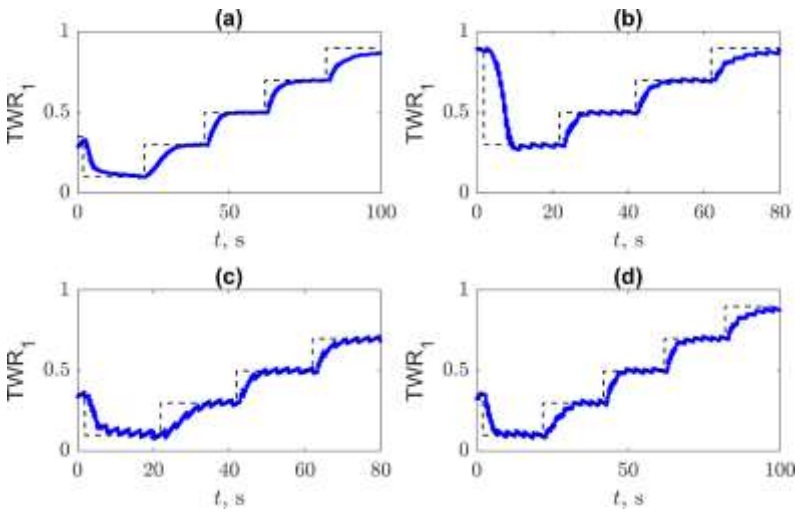

Fig 18. Measured TWR_1 from the adaptive control reference tracking experiments at different excitation frequencies: (a) – 1000 Hz, (b) – 2000 Hz, (c) – 2500 Hz, and (d) – 3000 Hz. Solid line – Measured TWR_1. Dashed line – Reference TWR_1.

The reference tracking results are shown in Fig 18. At all frequencies, the suggested control schematic results in a desirable steady-state error between the TWR_{ref} and TWR_1 and a fast convergence time compared to the transient waves' settling time. Some jitter is observed in the steady-state response; this becomes more visible at higher frequencies. The jitter may be removed by updating the controller time or gains at the higher amplitudes or using a more sophisticated version of control parameters updating such as the leaky-LMS[44].

Based on the model-based control results, it is concluded that the suggested control can be implemented on impedance tubes to increase the excited modal amplitudes' variability. By relying on this control schematic, one can set the modal TWR ratio obtained at each measurement and ensure that the acoustic parameter identification procedure will be well-conditioned.

V. CONCLUSIONS

In this work, an adaptive control method capable of controlling waves along elastic wavetube was developed. The capability to control the modal wave dynamics in an air-filled impedance tube using the suggested impedance control schematic has been demonstrated numerically and experimentally. The developed control method is composed of an observer-based controller. The observer estimates the modal TWR by employing the recursive MC-LMS model-based method. The tracking error-function norm is minimized using an adaptive gradient-descend approximation. The control strategy allows one to manipulate a chosen mode's dynamics at will while ensuring that the controlled parameters remain bounded by introducing a periodic extension of a predetermined parameter region. In addition, since the system is stable in the parametrized region, closed-loop stability is ensured.

Different methods to approximate the modal traveling wave ratio gradient were compared based on a numerical simulation. It was found that a zero-order approximation is comparable to both the finite difference approximation and the optimum seeking perturbation.

Being able to control the standing and traveling proportions of the pressure waves, one can overcome imperfections in the experimental system so that the impedance of a tested target can be accurately derived. Furthermore, the control algorithm can be adjusted for any frequency in a chosen region, despite the presence of multiple modes exhibiting dispersive behavior.

References

[1] ASTM E-1050, Standard Test Method for Impedance and Absorption of Acoustic Materials using a Tube two Microphones and a Digital Frequency Analysis System, Am. Soc. Test. Mater. **C**, 1-12 (1998).

[2] ASTM E-2611, Standard Test Method for Measurement of Normal Incidence Sound Transmission of Acoustical Materials Based on the Transfer Matrix Method 1, Annu. B. ASTM. Stand. **I**, 1-14 (2011).

[3] B. H. Song and J. S. Bolton, "A transfer-matrix approach for estimating the characteristic impedance and wave numbers of limp and rigid porous materials," J. Acoust. Soc. Am. **107**(3), 1131-1152 (2000).

[4] J. P. Dalmont, "Acoustic impedance measurement, Part I: A review," J. Sound. Vib. **243(**3), 427-439 (2001).

[5] V. A. Del Grosso, "Analysis of multimode acoustic propagation in liquid cylinders with realistic boundary conditions – Application to sound speed and absorption measurements," Acustica. **24**(6), 299-311 (1971).

[6] H. Sato, M. Lebedev, and J. Akedo, "Theoretical and experimental investigation of propagation of guide waves in cylindrical pipe filled with fluid," Japanese J. Appl. Physics, Part 1 Regul. Pap. Short Notes Rev. Pap. **45**(5 B), 4573-4576 (2006).

[7] Y. Vered, R. Gabai, and I. Bucher, "Waveguide dispersion curves identification at low-frequency using two actuators and phase perturbations," J. Acoust. Soc. Am. **146**(4), 2443-2451 (2019).

[8] L. D. Lafleur and F. D. Shields, “Low-frequency propagation modes in a liquid-filled elastic tube waveguide,” J. Acoust. Soc. Am. **97**(3), 1435-1445 (1995).

[9] K. Baik, J. Jiang, and T. G. Leighton, “Acoustic attenuation, phase and group velocities in liquid-filled pipes: Theory, experiment, and examples of water and mercury,” J. Acoust. Soc. Am. **128**(5), 2610-2624 (2010).

[10] R. S. Langley, “On the Modal Density and Energy Flow Characteristics of Periodic Structures,” J. Sound Vib. **172**(4), 491-511 (1994).

[11] Y. Vered and I. Bucher, “Experimental multimode traveling waves identification in an acoustic waveguide,” Mech. Syst. Signal Process. **153**, 107515 (2021).

[12] L. Feng, “Acoustic Properties Of Fluid-filled Elastic Pipes,” J. Sound Vib. **176**(3), 399-413 (1994).

[13] I. Bucher, “Estimating the ratio between travelling and standing vibration waves under non-stationary conditions,” J. Sound Vib. **270**(1-2), 341-359 (2004).

[14] R. Gabai and I. Bucher, “Excitation and sensing of multiple vibrating traveling waves in one-dimensional structures,” J. Sound Vib. **319**(1-2), 406-425 (2009).

[15] R. Gabai, D. Ilssar, R. Shaham, N. Cohen, and I. Bucher, “A rotational traveling wave based levitation device – Modelling, design, and control,” Sensors Actuators, A Phys. **255**, 34-45 (2017).

[16] I. Bucher, R. Gabai, H. Plat, A. Dolev, and E. Setter, “Experimental travelling waves identification in mechanical structures,” Math. Mech. Solids. **24**(1), 152-167 (2019).

[17] M. Åbom, “A note on the experimental determination of acoustical two-port matrices,” J. Sound Vib. **155**(1), 185-188 (1992).

[18] H. Bodén, “On multi-load methods for determination of the source data of acoustic one-port sources,” J. Sound Vib. **180**(5), 725-743 (1995).

[19] A. Holmberg, M. Åbom, and H. Bodén, “Accurate experimental two-port analysis of flow generated sound,” J. Sound Vib. **330**(26), 6336-6354 (2011).

[20] S. Sack and M. Åbom, “On Acoustic Multi-Port Characterisation Including Higher Order Modes,” Acta Acust. united with Acust. **102**(5), 834-850 (2016).

[21] M. L. Munjal, Acoustics of Ducts and Mufflers with Application to Exhaust and Ventilation System Design, John Wiley & Sons (1987).

[22] P. A. Nelson and S. J. Elliott, *Active Control of Sound*, Academic Press (1992).

[23] D. M. Kenney and P. H. Rogers, “A short water-filled pulse tube for the measurement of the acoustic properties of materials at low frequencies,” J. Acoust. Soc. Am. **103**(5), 3075 (1998).

[24] B. J. Brévart and C. R. Fuller, “Active control of coupled wave propagation in fluid-filled elastic cylindrical shells,” J. Acoust. Soc. Am. **94**(3), 1467-1475 (1993).

[25] S. J. Elliott and L. Billet, “Adaptive Control of Flexural Waves Propagating in a Beam,” J. Sound Vib. **163**(2), 295-310 (1993).

[26] A. H. Von Floton, “Traveling wave control for large spacecraft structures,” J. Guid. Control Dyn. **9**(4), 462-468 (1986).

[27] B. R. Mace, “Active control of flexural vibrations,” J. Sound Vib. **114**(2), 253-270 (1987).

[28] A. Minikes, R. Gabay, I. Bucher, and M. Feldman, “On the sensing and tuning of progressive structural vibration waves,” IEEE Trans. Ultrason. Ferroelectr. Freq. Control. **52**(9), 1565-1575 (2005).

[29] F. Giraud, C. Giraud-Audine, M. Amberg, and B. Lemaire-Semail, “Vector control method applied to a traveling wave in a finite beam,” IEEE Trans. Ultrason. Ferroelectr. Freq. Control. **61**(1), 147-158 (2014).

[30] W. J. O’Connor and M. Zhu, “Boundary-controlled travelling and standing waves in cascaded lumped systems,” Mech. Syst. Signal Process. **39**(1-2), 119-128 (2013).

[31] H. Habibi and W. J. O’Connor, “Wave-based control of planar motion of beam-like mass–spring arrays,” Wave Motion. **72**, 317-330 (2017).

[32] I. Peled, W. J. O’Connor, and Y. Halevi, “On the relationship between wave based control, absolute vibration suppression and input shaping,” Mech. Syst. Signal Process. **39**(1-2), 80-90 (2013).

[33] Y. Halevi, “Control of Flexible Structures Governed by the Wave Equation Using Infinite Dimensional Transfer Functions,” J. Dyn. Syst. Meas. Control. **127**(4), 579-588 (2005).

[34] R. Gabai and I. Bucher, “Spatial and temporal excitation to generate traveling waves in structures,” J. Appl. Mech. Trans. ASME. **77**(2), 1-11 (2010).

[35] L. Sirota and Y. Halevi, “Fractional order control of the two-dimensional wave equation,” Automatica. **59**, 152-163 (2015).

[36] P. F. Musgrave, V. V. N. S. Malladi, and P. A. Tarazaga, “Generation of traveling waves in a 2D plate for future drag reduction manipulation,” in Special Topics in Structural Dynamics, **6**. Springer, 129-138 (2016).

[37] S. Davis, R. Gabai, and I. Bucher, “Realization of an automatic, contactless, acoustic levitation motor via degenerate mode excitation and autoresonance,” Sensors Actuators A. Phys. **27**, 34-42 (2018).

[38] Y. Vered, R. Gabai, and I. Bucher, “Dispersion based reduced-order model identification and boundary impedance control in a weakly coupled impedance tube,” Proc. Mtgs. Acoust. **39**, 045005 (2019).

[39] M. Bouchard and S. Quednau, “Multichannel recursive-least-square algorithms and fast-transversal-filter algorithms for active noise control and sound reproduction systems,” IEEE Trans. Speech Audio Process. **8**(5), 606-618 (2000).

[40] P. C. Hansen, “Analysis of Discrete Ill-Posed Problems by Means of the L-Curve,” SIAM Rev. **34**(4), 561-580 (1992).

[41] P. C. Hansen, V. Pereyra, G. Scherer, *Least Squares Data Fitting with Applications*, Johns Hopkins University Press (2012).

[42] Y. Vered and I. Bucher, “Adaptive model-based control of boundary impedance in an acoustic impedance tube,” Proc. Mtgs. Acoust. **42**, 045004 (2020).

[43] B. Widrow and S. D. Stearns, *Adaptive Signal Processing*, Prentice Hall (1985).

[44] S. J. Elliott, *Signal Processing for Active Control*, Elsevier (2001).

[45] K. B. Ariyur and M. Krstic, *Real-Time Optimization by Extremum-Seeking Control*, John Wiley & Sons (2003).

[46] K. Baik, J. Jiang, and T. G. Leighton, “Acoustic attenuation, phase and group velocities in liquid-filled pipes III: Nonaxisymmetric propagation and circumferential modes in lossless conditions,” J. Acoust. Soc. Am. **133**(3), 1225-1236 (2013).